Heavily vanadium-doped LiFePO4 olivine as electrode material for Li-ion aqueous rechargeable batteries

To cite this article before publication: Milica Vujković *et al* 2024 *Mater. Res. Express* in press https://doi.org/10.1088/2053-1591/ad3463

Heavily vanadium-doped $LiFePO_4$ olivine as electrode material for Li-ion aqueous rechargeable batteries

Milica Vujković[1,2*], Maja Popović[3], Maria Čebela[3], Dragana Jugović[4]

[1] University of Belgrade - Faculty of Physical Chemistry, Studentski trg 12-14, 11158, Belgrade, Serbia
[2]Center for Interdisciplinary and Multidisciplinary Studies, University of Montenegro, Podgorica, Montenegro
[3] "Vinča" Institute of Nuclear Sciences—National Institute of the Republic of Serbia, University of Belgrade, Mike Petrovića Alasa 12-14, 11351 Belgrade, Serbia
[4] Institute of Technical Sciences of SASA, Knez Mihajlova 35/IV, 11158 Belgrade, Serbia

Since $LiFePO_4$ batteries play a major role in the transition to safe, more affordable and sustainable energy production, numerous strategies have been applied to modify LFP cathode, with the aim of improving its electrochemistry. In this contribution, a highly vanadium-doped $LiFe_{0.9}V_{0.1}PO_4$/C composite (LFP/C-10V) is synthesized using the glycine combustion method and characterized by X-ray diffraction (XRD), X-ray photoelectron spectroscopy (XPS), Thermogravimetry Differential Thermal Analysis (TGDTA) and Cyclic Voltammetry (CV). It is shown that 10wt.% of vanadium can substitute Fe positions, thus decreasing unit cell volume, which is followed by generation of $Li_3V_2PO_4$ traces, as detected by CV. High vanadium doping does not change the carbon content in the composite (≈ 13 wt.%) but improves its electronic conductivity and electrochemical performance in both aqueous and organic electrolytes. The reversibility and current response are increasing following the trend: LFP/C, LFP/C -3mol%V, LFP/C - 5mol % and LFP/C-10 mol %. The best specific capacity is obtained for the most highly doped olivine, which exhibits a reversible process at 1 mV s^{-1} in an aqueous electrolyte, thus showing a peak-to-peak distance of 56 mV. The high capacity of LFPC-10V is measured in both $LiNO_3$ and $NaNO_3$ electrolytes amounting to around 100 mAh g^{-1} at 20 mV s^{-1}. Still, the material is only stable in $LiNO_3$ electrolyte, making it more suitable for Li than Na-ion aqueous rechargeable batteries.

Keywords: $LiFePO_4$, vanadium doping, Li-ion batteries, Na-ion batteries, aqueous electrolyte,

*Corresponding author: Milica Vujković, Principal Research Fellow

University of Belgrade - Faculty of Physical Chemistry

Studentski trg 12–14, 11158 Belgrade, Serbia

E–mail address: milica.vujkovic@ffh.bg.ac.rs;

1.Introduction

Since Sony released the first Li-ion battery, the number of scientific papers and patents has grown exponentially [1], which has resulted in its improved performance and Nobel prize in 2019. The current energy density of around 300 Wh kg^{-1} has enabled Li-ion batteries not only to rule high technology, but also integrate into renewable energy infrastructure and penetrate the market of electric vehicles. However, there is still room for improvement in energy density to reach theoretical values for some battery systems, based on the mass of all integrated components [2]. Therefore, one part of the research is strongly focused on increasing the energy density of Li-ion batteries by developing high-capacity materials and/or highly conductive electrolytes [3,4] mostly relying on solid-state, metal-air, and metal-sulfide batteries, while the other part puts the accent more on safety and sustainability aspects than on energy improvement [5–8] .

$LiFePO_4$ (LFP) batteries are considered one of the best options when it comes to addressing issues of safety, sustainability and environmental suitability. Their combination, with an aqueous system, makes the battery system "ideal" from an ecological and non-toxic point of view. Since the discovery of $LiFePO_4$ (LFP) by John Goodenough [9,10], many strategies have been developed in the literature to improve its performance. These include the synthesis of olivine nanoparticles [11], their carbon coating and anchoring with CNT or RGO [12–14], doping with various cations and anions [15–17], etc. Vanadium substitution into olivine was found to be an effective strategy to boost its electrochemical performance[16,18–21]. Although there were initial discrepancies [16,18,21–23]as to whether the vanadium ion occupied the cationic or anionic position of $LiFePO_4$, most authors agreed that vanadium preferentially replaced Fe positions [21,23–25], while occupation of Li sites was also possible [26]. By occupying Fe positions, vanadium increases the effective Li^+ cross-sectional area of the LiO_6 octahedral face [25] and lowers the energetic barrier for Li ion diffusion through a one-dimensional olivine channel [27]. Furthermore, secondary phases such as VO_2, $Li_3V_2(PO_4)_3$ … are usually observed as an accompanying phase of V-doped LFP, especially at higher doping levels [21,23], which may have a positive effect on the electronic conductivity and hence electrochemical performance. The phase composition of V-doped $LiFePO_4$ strongly depends on the amount of doped vanadium [23].

Our group has focused a lot on the vanadium doping strategy [28,29], where we showed that the performance of $LiFePO_4$/C (LFP/C), synthesized by the glycine-nitrate combustion process, can be successfully improved by doping with low vanadium fraction of 3 and 5 mol%, in both organic and aqueous electrolytes. Namely, incorporation of vanadium into Fe sites is capable of increasing the electronic conductivity of LFP/C and extending Li-O bonds, thereby promoting the diffusion of Li-ions. The aim here was to investigate the influence of a high level of vanadium doping on the structure and electrochemical behavior of the synthesized olivine, targeting the composition of $LiFe_{0.9}V_{0.1}PO_4$/C. Therefore, heavily vanadium-doped $LiFePO_4$, more specifically $LiFe_{0.9}V_{0.1}PO_4$/C (LFP/C-10V), was synthesized by our developed gel-combustion procedure and subjected to structural analysis and electrochemical testing in both Li- and Na-containing aqueous electrolytes [28–30]. The results are discussed by comparing the electrochemical behavior of LFP/C with different vanadium doping levels (3, 5 and 10 mol %). The insertion behavior of lithium and sodium was also compared. While the influence of high vanadium doping level on the

electrochemical performance of LFP in an organic electrolyte has been the subject of several studies [21,23], no similar reports have been found regarding the electrochemical behavior in an aqueous electrolytic medium. This way we complete the puzzle relying on the electrochemistry of V-doped $LiFePO_4$. Besides, there is no report on the use of glycine combustion synthesis for producing highly doped LFP. The study also shows that 10 mol% of vanadium can be successfully incorporated into an olivine lattice at higher temperatures, via a gel-combustion route. Such high vanadium doping in LFP/C is an effective way to improve performance, even beyond that achieved with a low doping level. A novel LFP-based cathode, with an excellent high-rate performance, is proposed for aqueous rechargeable Li-ion batteries.

2. Experimental

$LiFe_{0.9}V_{0.1}PO_4$/C composite was synthesized according to our developed procedure [28,30]. Briefly, stoichiometric amounts of $LiNO_3$ (Alfa Aeser), $FeC_2O_4x2H_2O$ (Sigma Aldrich), $NH_4H_2PO_4$ (Merck) and NH_4VO_3 (Merck) were mixed with water, glycine (the molar ratio of glycine to nitrate was 2:1) and malonic acid (60 wt.% of the theoretical olivine mass) to evaporate at 80 ◦C using a magnetic stirrer. The obtained gelled precursor was transferred to an oven at 190 ^oC to cause the auto-combustion process, resulting in a flocculent product that was further heated in a quartz tube furnace first at 350 ^oC (for 3h) and then at 750 ^oC for 6h, in a reducing atmosphere of $Ar/5H_2$.

X-ray powder diffraction was measured on the Philips PW 1050 diffractometer, equipped with Nickel-filtered Cu-$K\alpha_{1,2}$ radiation, in the 2 theta range from 10 to 120°. The scanning step was 0.02° and the counting time was 12 s per step.

The composite sample was subjected to thermogravimetric analysis using the Thermobalance TA SDT Model 2090. The experimental setup involved controlled heating at a programmed rate under an air atmosphere to allow carbon combustion. During the experiment, the change in mass as a function of temperature was continuously recorded.

The electrical conductivity of the same sample was assessed using an AC bridge Wayne Kerr B224, operating at a fixed frequency of 1 kHz. This frequency is commonly employed in electrical conductivity measurements to ensure consistent testing conditions. LFP/V-10V powder was subjected to compaction to form a pellet of uniform size and density. The compaction process was controlled rigorously to maintain consistency in pellet dimensions.
To achieve reliable electrical contact, the contact surfaces of the prepared pellet were evenly coated with a layer of high-conductivity silver paste. The coating process aimed at complete coverage of the pellet surfaces, ensuring minimal risk of electrical discontinuities as well as stable and durable electrical contact.

XPS analysis of the samples was carried out on SPECS Systems with XP50M X-ray source for Focus 500 and PHOIBOS 100 energy analyzer using a monochromatic Al Kα X-ray source (1486.74 eV) at 12.5 kV and 16 mA. The sample was fixed onto an adhesive copper foil to provide strong mechanical attachment and good electrical contact. During the measurement the base

pressure in the system was below 5×10-9 mbar. The XPS spectra were collected by SpecsLab data analysis software.

Electrochemical measurements were measured in a three-electrode cell. For aqueous electrolyte (6M $LiNO_3$ and 6M $NaNO_3$), the cell was composed of working electrode (LFP/C-10V sample attached to the conductive support), Pt foil as a counter electrode and reference saturated-calomel electrode (SCE). Both Cyclic voltammetry (CV) and Chronopotentiometry (CP) measurements were performed using Gamry 1010E Potentiostat/Galvanostat. For organic electrolyte (1M $LiClO_4$/PC), the cell was composed of LFP/C-10V as a working electrode and lithium foil as both counter and reference electrodes (assembled in Ar-filled glove box). CV measurement in an organic electrolyte was performed using Potentiostat PAR A.

The working electrode was prepared for all measurements by mixing active powder with PVDF binder dispersed in N-methyl-pyrrolidone and Carbon Black additive (Cabot Vulcan® XC72R) to form a slurry (75:5:20 wt%, respectively), which is further attached to the conductive glass carbon (for the measurements in an aqueous electrolyte) or Pt foil (for the measurements in an organic electrolyte). Total electrode loading for all measurements was about 4-5 mg cm^{-2}. CV measurement in an organic electrolyte (1M $LiClO_4$) was performed to characterize the sample in terms of identifying secondary phase.

3. Results and discussion

3.1 Structural, surface, thermal and conductive behavior

X-ray powder diffraction pattern (Figure 1) matches the pattern of $LiFePO_4$ with olivine structure (PDF2 # 40-1499), with no obvious peaks that could be assigned to other crystalline phases. Therefore, it was natural to assume that the vanadium ions from the precursor solution are incorporated either in the olivine structure of $LiFePO_4$ or compose a non-crystalline phase. Internal carbon is in an amorphous form and contributes to the background. The crystal structure refinement, based on the Rietveld full profile method [31], was done using the Koalariet software [32]. The refinement was done in the orthorhombic Pnma (D_{2h}^{16}) space group in the olivine type where Li^+ ions occupy 4*a* [0,0,0] positions with local symmetry $\bar{1}$; Fe^{2+} and P^{5+} ions occupy two nonequivalent 4*c* crystallographic positions [x,1/4,z] with local symmetry *m*; O^{2-} ions occupy three different crystallographic positions: additional two 4*c* positions and one general 8*d* position [x,y,z] with local symmetry 1. The results of the refinement are listed in Table 1, while its graphical interpretation is given in Figure 1.

During the refinement, it was presumed that vanadium ions V^{3+} only occupy the iron site. This is justified by the fact that V^{3+} ions are comparable in size to iron ions and are much larger than phosphorous ions [33]. The calculated occupation of the iron site by vanadium ions matches the iron/vanadium ratio in the precursor solution (9:1), which implies that all vanadium ions are incorporated in the olivine phase. Consequently, lattice parameters (Table 1) are smaller than the lattice parameters of the undoped powder [28]. In our previous paper [28], the cell volume of olivine was found to decrease upon low vanadium doping of 3mol% ($LiFe_{0.95}V_{0.05}PO_4$/C) and 5mol% ($LiFe_{0.95}V_{0.05}PO_4$/C), which is consistent with the literature [18,23,34]. However, the linear trend of further decreasing a volume cell up to 10 mol% is not observed. At higher doping

concentrations of vanadium, there is a deviation from Vegard's rule, which is quite common because Fe^{2+} and V^{3+} are not isomorphous ions.

Whittingham at al [16] indicated that the maximal amount of vanadium, that can be incorporated into LFP, is 10 mol% but only at a low temperature of 550 ºC. It is shown here that ≈10 wt.% of vanadium could still be incorporated into the olivine lattice, upon its heating at 750 ºC under reducing atmosphere. The carbon presence may catalyze the doping process and allow a higher amount of incorporated vanadium. Additionally, cyclic voltammetry still identifies $Li_3V_2(PO_4)_2$ (LVP) traces in the synthesized sample (see below), which could not be detected by XRD. Therefore, ≈10 mol% can be regarded as the limiting concentration of vanadium, capable of doping into LFP/C under these synthesis conditions.

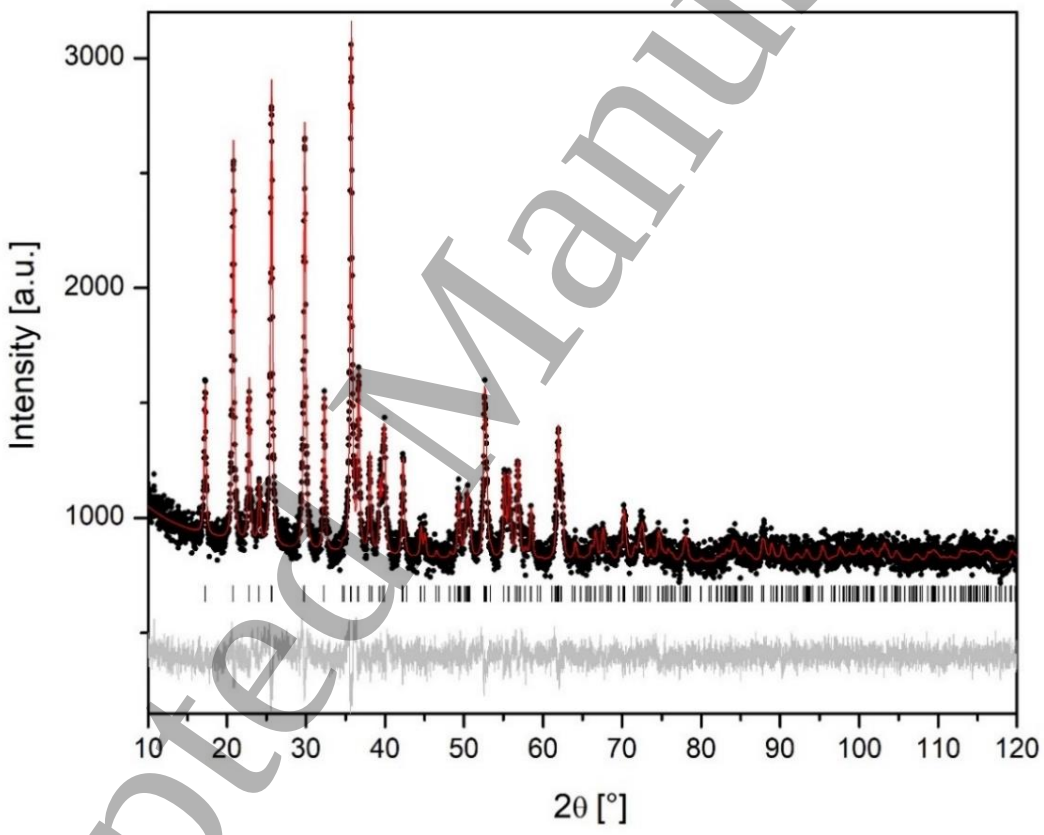

Figure.1 X-ray diffraction data of the investigated sample. The observed (.), calculated (−), and the difference between the observed and calculated (bottom). Vertical markers below the diffraction patterns indicate positions of possible Bragg reflections for olivine type $LiFePO_4$.

Microstructural parameters, mean crystallite size and microstrain, imply that the given synthesis procedure is suitable for obtaining powder with small crystallite size (50 nm) of low distortion (Table 1). Doping with vanadium causes the contraction of both P-O and Fe-O bonds, the elongation of the Li-O bond (Table S1) and reduces an anti-site defect. Such a structure should be favorable for lithium-ion diffusion. Anti-site defect is an intrinsic defect of an olivine phase in which lithium ions (on M1 site) and iron ions (on M2 site) are interchanged. This is recognized as

a critical problem for lithium diffusion through one-dimensional channel along [101] direction, which leads to smaller capacity [35]. Iron ions positioned on the lithium site can "block" the whole lithium channel and prevent lithium motion. Doping with vanadium prevents cation mixing (anti-site defect) and enables better utilization of the material.

Table 1. The results of the Rietveld refinement

Paramaters	$LiFe_{0.9}V_{0.1}PO_4/C$	$LiFePO_4/C$ [ref]
Lattice parameters (Å)	a = 10.3002(8)	a = 10.3270(9)
	b =5.9947(4)	b = 6.0090 (5)
	c = 4.6992(4)	c = 4.6968(5)
Primitive cell volume ($Å^3$)	V= 290.16 (4)	V= 291.46 (5)
Microstrain (%)	0.06(4)	0.20(4)
Fe site occ. by V	0.10 (9)	-
Li site occ. by Fe	0.007 (9)	0.022(9)
R factor (%)	Rwp = 4.35	Rwp = 5.85

To characterize the surface of the synthesized sample, XPS measurement was performed. In Fig.2 we present survey XPS spectra (Fig.2a) together with high-resolution XPS spectra of Fe3p, Li1s, Fe2p and V2p lines taken from the LFP/C-10V sample. XPS core line at around 56eV (Fig.2b) can be deconvoluted into two components, one at a higher binding energy, originating from Fe3p, and other at a lower, belonging to Li1s. Higher intensity of Fe3p is expected due to its greater relative atomic sensitivity than that of Li1s [35]. The characteristic $Fe2p_{3/2}$ and $Fe2p_{1/2}$ core-level photoelectron lines, positioned at 710.9 eV and 724.2 eV, (Fig.2c), with two satellite peaks at higher binding energies (716 eV and 729 eV), can be attributed to Fe^{2+} state [23,34,36–38]. The V2p core-level line with the V2p3/2 and V2p1/2 doublets, located at 517 and 524.3 eV, respectively is shown in Fig. 3d. It is well-known that vanadium can exist in different valence state (V^{3+}, V^{4+} or V^{5+}) [39] where the position of the $V2p_{3/2}$ photoelectron line is within 515-517 eV binding energy range. The same oxidation state can vary by 0.5 eV for the same type of compound [39], while the average vanadium oxidation state in V-doped LFP (for example 3.2+) is also possible [22,24], making the assignment problematic. If we go through the literature on V-doped LFP, we can see that some authors [23,40] assigned main V lines of LFVP to the V^{4+} state referring to XPS spectrum of VO_2 [23,40], while others still attributed the same bands to the 3+ oxidation state thus following XPS of $Li_3V_2PO_4$ [19,36,41]. There is also a study that assigns these V2p bands to V^{5+} [42]. Therefore, due to the large spread of the reported data, the vanadium oxidation state of LFP/C-10V cannot be identified with certainty using the XPS analysis. The broadness of the stronger V2p line towards lower binding energies (Fig.2d) may be the consequence of different local environment of vanadium in the doped sample, which is more pronounced by the presence of surface $Li_3V_2PO_4$ and its interface with LFP/C. Based on the structural analysis, we assume that highly intensive line (517eV) could be related to V^{3+} oxidation state in vanadium-doped $LiFePO_4$, while its shoulder at 515eV could originate from the same state in LVP phase.

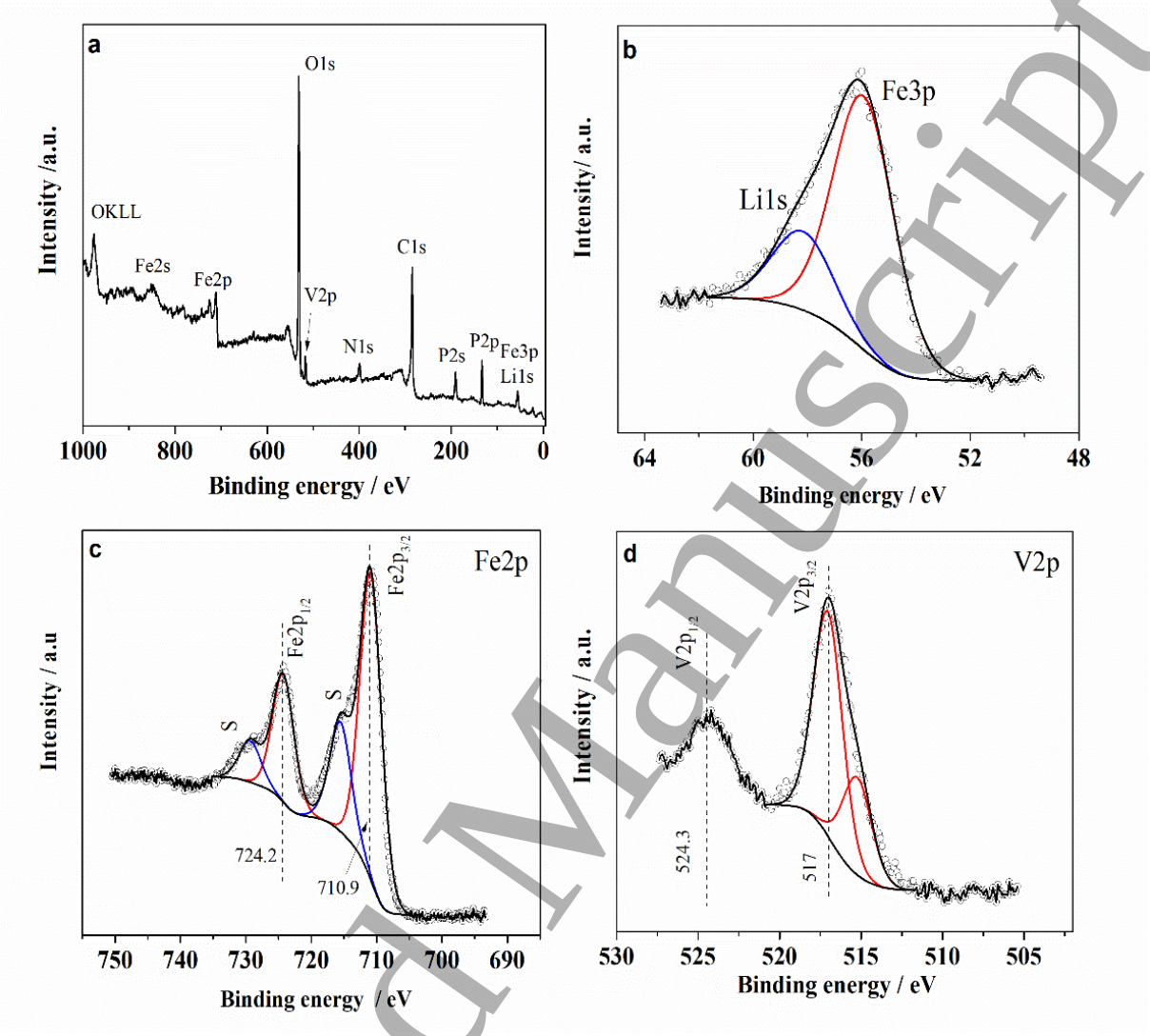

Figure.2 XPS survey spectrum (a) and high-resolution XPS core level lines of Fe3p, Li1s (b), Fe2p (c) and V2p (d) for LFP/C-10 V.

The carbon content in the LFP/C-10V sample, determined thermogravimetrically (Fig.S2), was found to be similar to the one for the undoped sample, amounting to ≈ 13 wt. %. Furthermore, the electrical conductivity of highly vanadium-doped LFP/C amounts ≈ 2 $\cdot 10^{-2}$ S/cm, which is one order of magnitude higher than published values obtained for pristine LFP/C (≈ 1.43 x 10^{-3} S cm^{-1}) and $LiFePO_4$ with low vanadium content (≈ 1.68 x 10^{-3} for $LiFe_{0.97}V_{0.03}PO_4$/C and ≈ 1.70 x 10^{-3} S cm^{-1} for $LiFe_{0.95}V_{0.05}PO_4$/C) [28]. Since the carbon content, in the composite, remained unchanged after a high level of vanadium doping, one can conclude that the improvement of the electronic conductivity can be related to vanadium doping.

3.2. Electrochemical behavior

3.2.1 CV characterization in Li-based aqueous and organic electrolyte

The initial cyclic voltammograms of LFP/C-10V powder, measured in an aqueous $LiNO_3$ electrolyte at 20 mV s^{-1}, are shown in Figure 3,a,b. A vaguely defined anodic peak in the first cycle and an initial increase in CV until stabilization can be identified. Since the first anodic peak of LFP/C-10 V measured in the organic electrolyte (Fig.3c) is more pronounced, we can rule out lithium deficit as the source of the poor initial response in an aqueous electrolyte. The reason may be a better initial wetting of the composite in an organic electrolyte than in an aqueous one. Even so, the stabilized CV response and peak-to-peak separation in the aqueous electrolyte are significantly better than in an organic one, which indicates a faster Li ion insertion/deinsertion kinetics in an aqueous electrolyte, driven by its better ionic conductivity. Furthermore, the initial CV rise is usually correlated with slower penetration of Li^+ ions through amorphous carbon layer and/or intrinsic phenomena such as particle size reduction during cycling [43].

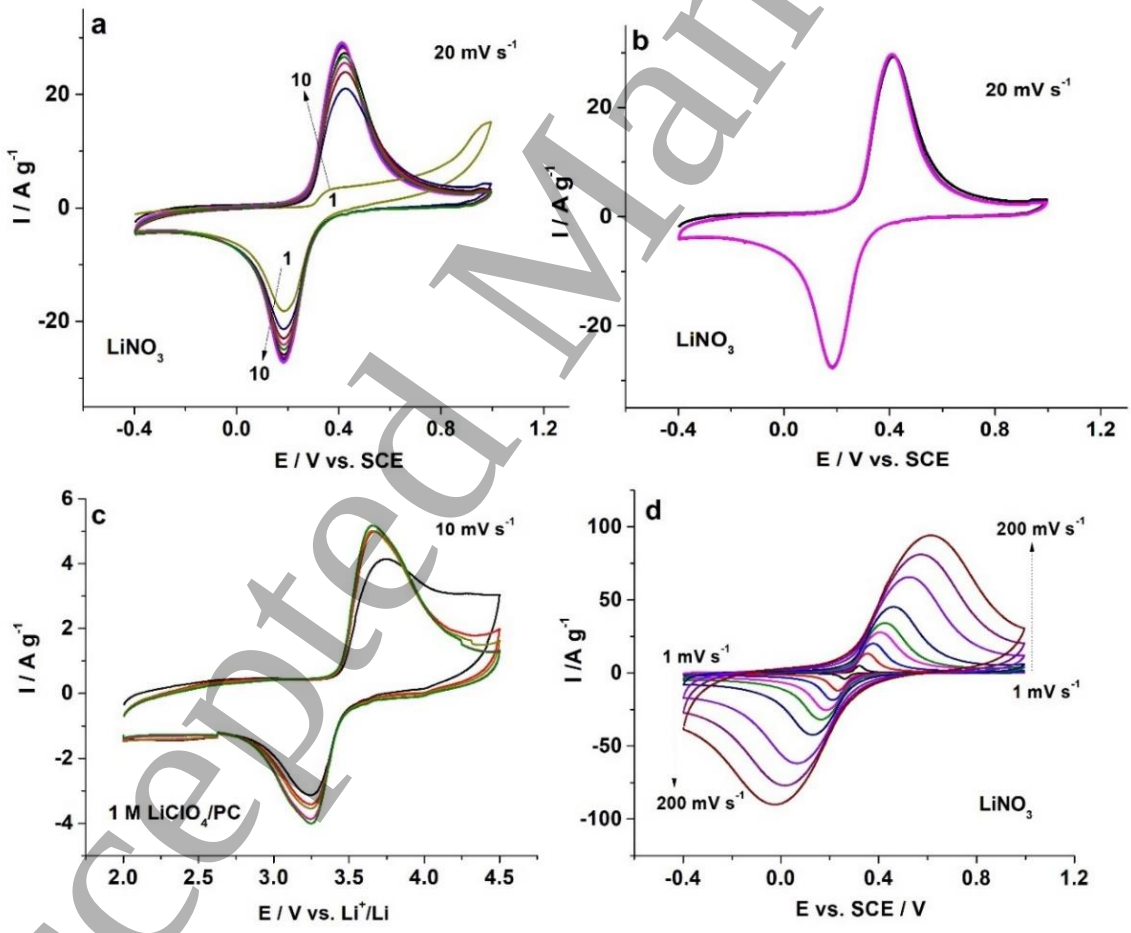

Figure 3. CVs of LFP/C-10V measured in 6 M $LiNO_3$ aqueous electrolyte at a scan rate of 20 mVs^{-1} during the first 20 cycles (a,b) and 1M $LiClO_4$/PC at a scan rate of 10 mV s^{-1} during the first five cycles (c). CV of LFP/C-10V in $NaNO_3$ at different current rates from 1 to 200 mV s^{-1} (d).

Characteristic redox pair of olivine (positioned at 0.18/0.4 vs. SCE at 20 mV s^{-1}) corresponding to the deintercalation/intercalation process, followed by $LFePO_4/FePO_4$ phase transition [9,10], can be recognized. The peaks are well-defined, not only at lower, but also at higher scan rates up to the atypical value of 200 or 300 mV s^{-1} (Fig.3d and Fig. S1), thus showing high current response and a small peak potential separation. The distance between peaks, expressed as $\Delta E/2$, amounts to 28 mV for 1 mVs^{-1}, which corresponds to a fully reversible process (Fig.4a). This indicates the high quality of the LFP sample with extremely fast and stable electrochemical reactions in an aqueous medium.

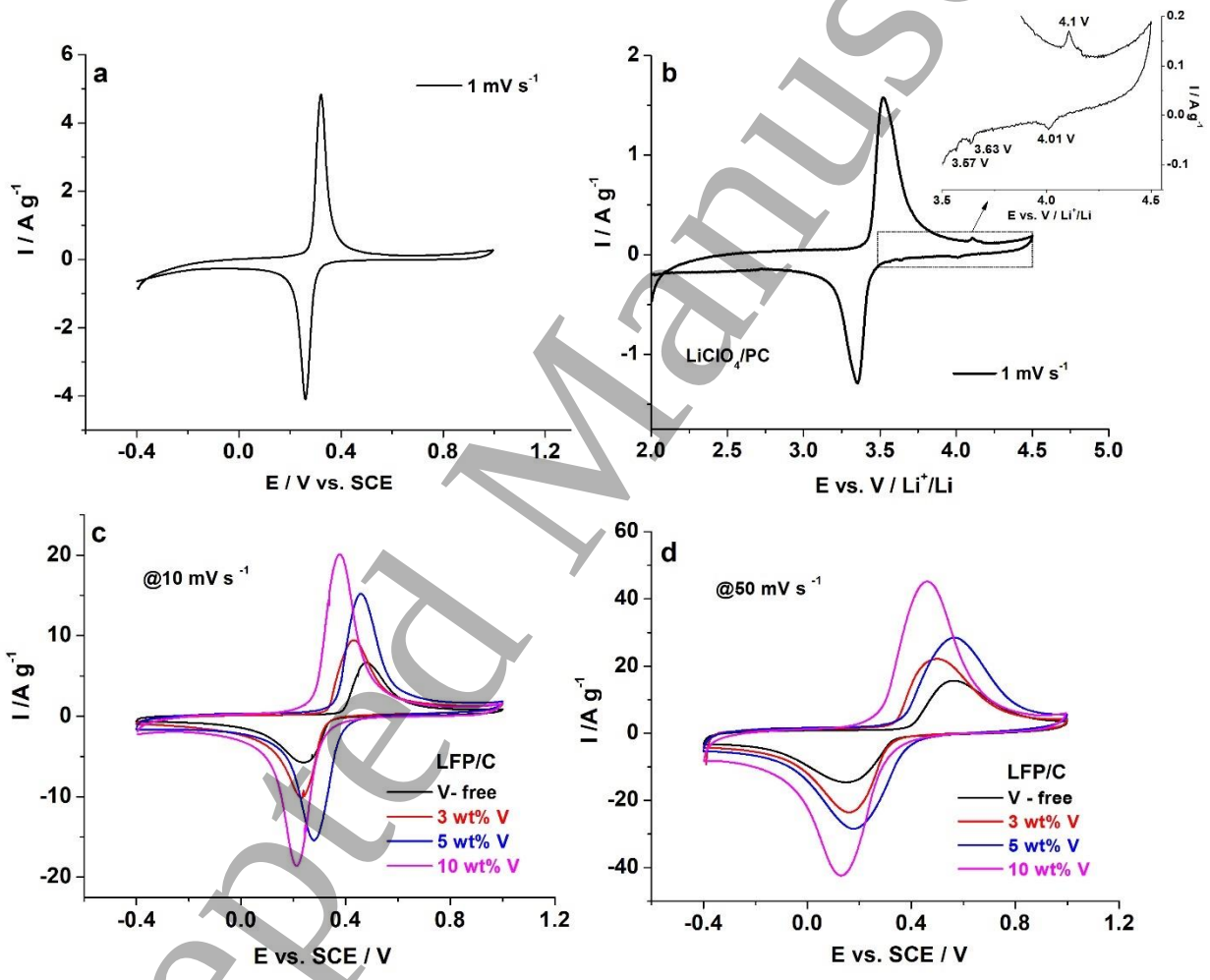

Figure.4 CVs of LFP/C-10V measured in 6M $LiNO_3$ (a) and 1M $LiClO_4$/PC (b) at 1 mV s^{-1}; Comparative CVs of LFP/C with (3, 5 and 10 wt.%) and without vanadium, measured in $LiNO_3$ at a common scan rate of 10 mVs^{-1} (c) and 50 mV s^{-1} (d).

Secondary phases in LFP/C-10V are not detected by XRD because they are not formed during LFP synthesis at 750 °C, or are below the detection limit of this method. To solve this issue, CV of the powder was also measured in an organic electrolyte at 1 mVs^{-1} (Fig.4b), since some accompanying

phases such as $Li_3V_2(PO_4)_2$, $LiVOPO_4$, VO_2 can be identified at lower scan rates due to their highly conductive behavior. In addition to the main redox pair of olivine, we can notice very small redox peaks (4.0/41 V vs. Li^+/Li and two cathodic ones at 3.63 and 3.57 V vs. Li^+/Li) corresponding to the V^{3+}/V^{4+} redox process of $Li_3V_2(PO_4)_2$[21,23]. The appearance of this phase at a high level of vanadium doping matches the literature data [21,23]. Namely, there was an excess of vanadium that migrated to the surface during heating and formed this phase. Since its content is very small, it did not affect the final $LiFe_{0.9}V_{0.1}PO_4$ composition determined by Rietveld analysis. This explains why the Fe_2P phase is not formed along LFP/C-10V phase, as observed in the case of low vanadium doping level [28]. It is confirmed that the amount of substituted vanadium at Fe sites determines not only the crystal parameters of LFP olivine lattice, but also the phase composition of doped LFP, particularly in terms of secondary phase appearance (usually inevitable during LFP synthesis), which can have a positive influence on electrochemistry. Here, LVP can contribute to LFP electronic conductivity [21,23] and therefore enhance its specific capacity.

CV change with the scan rate indicates the typical ohmic resistive behavior of the sample [44], based on the slopping straight line which can be drawn across the frontal sides of anodic and cathodic peaks, at different scan rates. The material behaves as an ohmic resistor, showing lower values of polarization resistance R (as a reciprocal of the slope of the straight line touching the peak fronts) when compared to a low doping level. The influence of heavy vanadium doping on LFP performance can be clearly seen in Fig.4c,d and Table 2. Highly doped LFVP/C exhibits the best current response among all V-doped samples, especially at higher scan rates. The trend of increasing current response and decreasing peak-to-peak potential separation follows the order LFP, LFP-3%V, LFP-5%V and LFP-10%V, thus confirming reversibility improvement upon vanadium doping.

Table 2. The peak-to-peak potential distance ((Ep,a − Ep,c)/2) at various scan rates calculated from cyclic voltammograms of LFVP-based samples in $LiNO_3$.

Scan rate /mV s^{-1}	$E_{p,a}$-$E_{p,c}$/2 (mV) for LFP/C			
	$LiFePO_4/C^{[ref]}$	$LiFe_{0.95}V_{0.05}PO_4/C^{[re]}$	$LiFe_{0.95}V_{0.05}PO_4/C^{[re]}$	$LiFe_{0.9}V_{0.1}PO_4/C$
1	55	39	29	**28**
5	89	75	66	**61**
10	120	96	90	**83**

By integrating cyclic voltammograms at different sweep rates, the specific capacity as the function of the scan rate was calculated and shown in Table 3. LFP/SC-10 V delivers the high specific capacity of around 100 mAh g^{-1} over a wide range (from 1 to 20 mV s^{-1}), with an excellent anodic/cathodic efficiency. The high value is retained even at 300 mV s^{-1}, amounting to an impressive 75/72 mA hg^{-1} for lithiation/delitiation. If the scan rate is expressed through C, the capacity of the synthesized composite reaches value of 70 mAg h^{-1} at an extremely high current of 423 C (charging in ≈ 8 s) 632 C (charging in ≈ 6 s). Accordingly, LFP/10 V material holds great potential as a cathode material for aqueous Li-ion rechargeable batteries. In our previous paper, we optimized the electrochemical performance of LFP/C with a low level of vanadium doping, using an aqueous electrolyte of $LiNO_3$. Then, LFP/C doped with 5 mol%V showed the best

performance. Herein, improved behavior of the heavily vanadium-doped sample was observed over 50 cycles of charge/discharge (Fig.S3).

To summarize, heavy vanadium doping of LFP significantly improves its charge storage performance in the aqueous electrolyte, especially at high current rates. Replacement of Fe sites by Vanadium makes Li-O bonds longer and reduces an anti-site defect, thus facilitating diffusivity of Li ions through the one-dimensional channel, while the improved electronic conductivity is achieved through both vanadium incorporation and $Li_3V_2(PO_4)_2$ formation. This way, both LFP bottlenecks, poor intrinsic ionic and electronic conductivity, have been overcome, enabling superior performance of the composite.

In general, the capacity fade of olivine is typical behavior in an aqueous solution due to side reactions of Fe (II) in LFP with oxygen-containing species in the electrolyte [45]. Stable behavior during consecutive cycling (Fig.S3) can be attributed to the high amount of carbon which prevents attack of oxygen species to the olivine particles and consequently their dissolution.

Table 3. The specific coulombic capacity calculated from CVs of LFVP/C measured in $LiNO_3$ electrolyte, at different scan rates.

Scan rate /mVs^{-1} (also expressed via ≈ C)	**Anodic capacity / mAh g^{-1}** (delithiation)	**Cathodic capacity/ mAh g^{-1}** (lithiation)
1 (2.6)	107	103
5 (12.9)	104	107
10 (25.7)	101	103
20 (51)	96	97
30 (76.6)	83	83
50 (128.5)	78	78
100 (211.7)	82 (85)*	80 (83)
150 (318)	76 (81)*	74 (80)
200 (423)	71 (79)*	69 (77)
300 (632)	62 (75)*	60(72)

* Capacities obtained from CVs (Fig.S1) with the iR compensation

3.2.2 CP measurements in $LiNO_3$ aqueous solution

To determine the capacity of the sample upon galvanostatic regime, the chronopotentiometry curves are measured over the stable potential interval of $LiNO_{3aq}$, at high current rates. As shown in Fig.5, charge/discharge plateaus (corresponding to $LiFePO_4 \leftrightarrow FePO_4$) are clearly defined, almost merging at a potential of ≈ 0.3 V vs. SCE upon passing of lower current densities (2 – 10 C). An insignificant separation between plateaus at lower current densities (2 – 10 C), more pronounced at higher currents (20-100 C), confirms a truly fast kinetics of lithium deintercalation/intercalation process of olivine in $LiNO_3$ aqueous solution.

Delithiation (charge curve) and lithiation (discharge curve) specific capacities are listed in Table 4. High values are registered at 2 C, amounting to ≈ 108 mAh g^{-1} for delithitation and ≈ 90 mAh g^{-1}, for lithiation, with a high retention of 100 C (57 and 47 mA h g^{-1}, respectively). The columbic

capacities calculated from CP are very similar to values obtained from cyclic voltammetry. Unlike CV, CP shows a slightly higher discharge/charge efficiency, due to a somewhat lower positive potential limit (1 vs. 1.2 V relative to SCE), which prevents the full oxidation process.

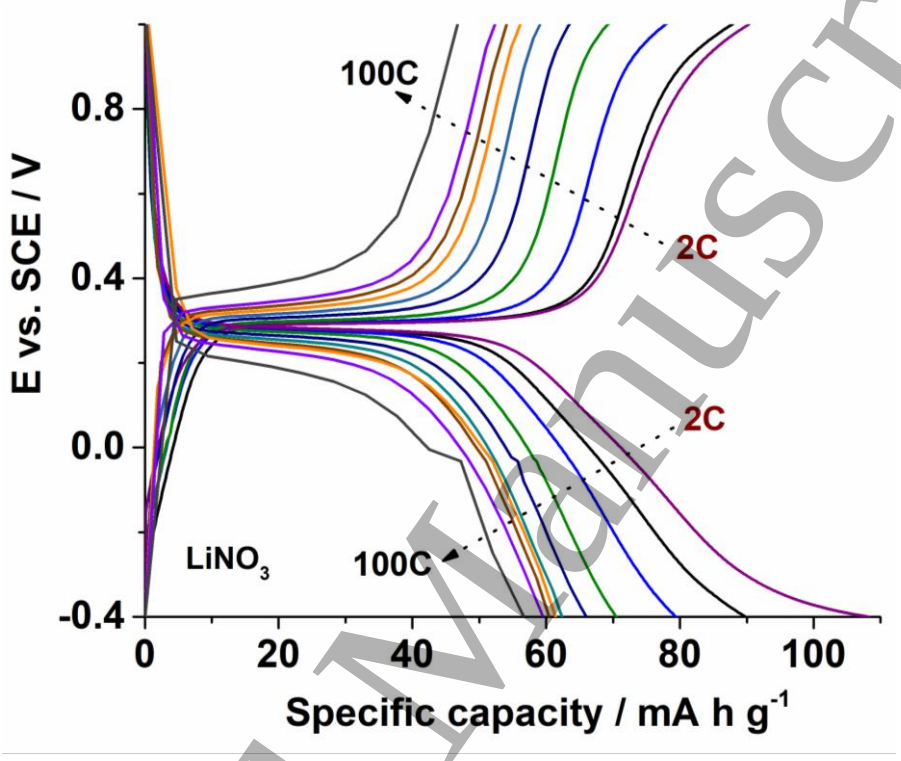

Figure.5 CP curves of LFP/C-10V measured in $LiNO_3$ aqueous electrolyte

Table 4. Delithiation/lithiation coulombic capacity calculated from CP curves of LFVP/C measured in $LiNO_3$ aqueous electrolyte, at different current rates expressed via theoretical capacity of LFP.

Current density via C (1C = 170 mAh g^{-1})	**Delithiation capacity / mAh g^{-1}** (charge CP curve)	**Cathodic capacity/ mAh g^{-1}** (discharge CP curve)
2	108	90
3	90	88
5	79	78
10	71	70
20	66	65
30	62	61
40	61	59
50	60	54
60	60	54
100	57	47

3.2.3. Li vs. Na insertion/deinsertion behavior

The highly doped composite was also examined in Na-containing aqueous electrolyte by cyclic Voltammetry (Fig.6). The first five cycles in $NaNO_3$ are shown in Fig.6a and indicate the typical Li-Na exchange of LFP [29,46,47]. The Li-Na exchange is achieved rapidly during the first five cycles at 20 mVs^{-1}, thus producing the $NaFePO_4$ phase, as confirmed through the shape of stabilized CV curves (Fig.6b). Simply, the exchange of typical CV shape of LFP (initial cycles) to CV shape of $NaFePO_4$ (stabilized cycles) is evidenced, thus confirming the Li-Na exchange process (governed by the applied scan rate). Namely, the stabilized CV is a typical voltammogram of sodium olivine form, where the observed redox peaks (two anodic and one cathodic) reflect $NaFePO_4$-$FePO_4$ phase transition, occurring via intermediate $Na_{0.7}FePO_4$ phase [29,47,48].

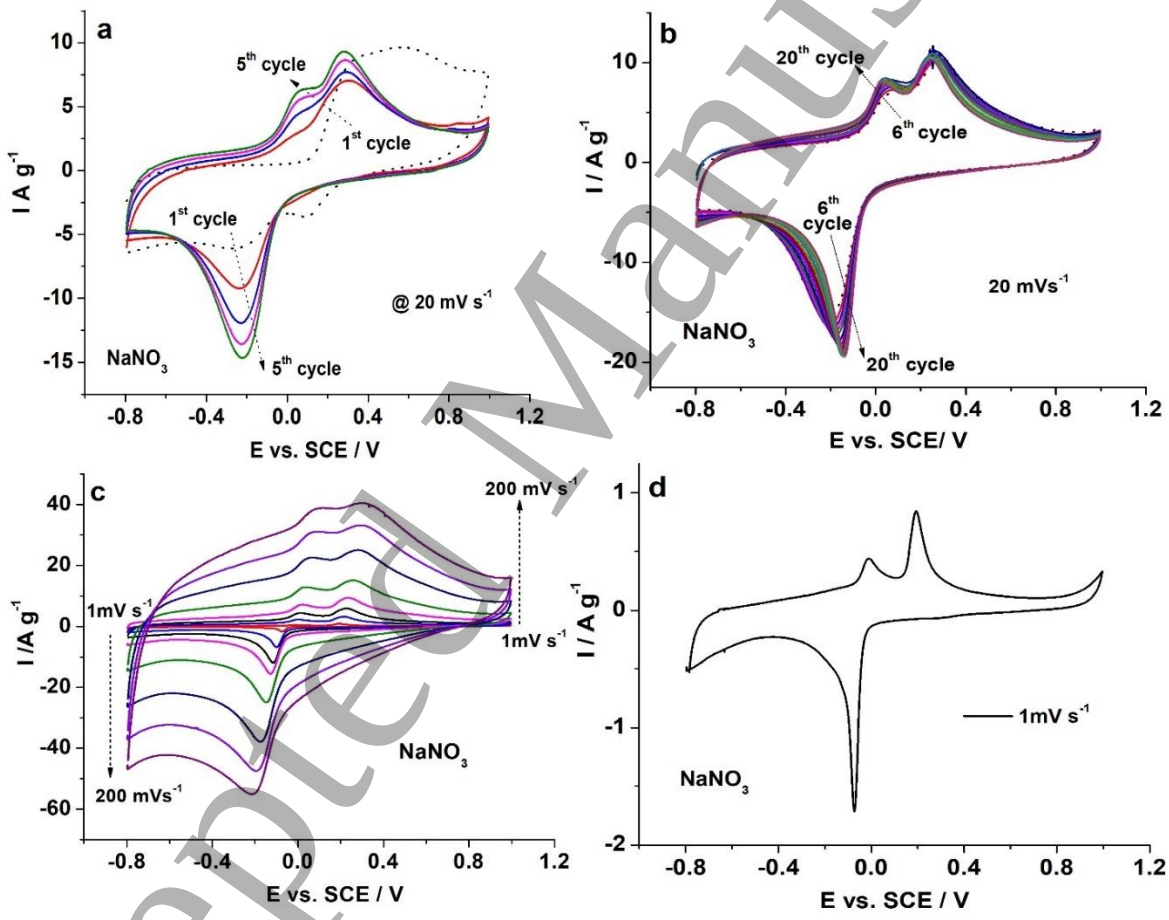

Figure 6. CVs of LFP/C-10V in $NaNO_3$ aqueous electrolyte: the first 5 cycles (a) and the next 20 cycles at 20 mVs^{-1} (b); Corresponding CVs at different scan rates (c) and 1mVs^{-1} (d).

After stabilizing CV at 20 mVs^{-1}, we first measured CV at lower scan rates up to 1 mV s^{-1} and then at higher ones up to 300 mVs^{-1} (Fig.6c). Well-defined peaks (one cathodic at -0.075 V vs. SCE and two anodic peaks at -0.0109 and -0.075 V vs. SCE) with small peak-to-peak separation are observed, as shown in Fig.6d. They become less defined at a higher scan rate, compared to the redox process involving lithium, which can be attributed to not only pseudocapacitance behavior

but also to material instability (Fig.7). Unlike lithium insertion/deinsertion process, which is quite stable during cycling over a wide range of scan rates, the current corresponding to sodium insertion /deinsertion decreases slightly after cycling at lower scan rates and even more upon higher scan rates (Fig.7a). This indicates a higher material potential for Li- than for Na-ion rechargeable batteries.

The storage capacity values of LFP/C-10 V for Na ions are listed in Table 4, while the comparative performance of LFP/C-10V in $LiNO_3$ and $NaNO_3$ can be best seen in Fig.7. Although the current height of LFPC-10V in $LiNO_3$ is significantly higher than that in $NaNO_3$ (Fig.7), the integrated parts of CVs in $LiNO_3$ and $NaNO_3$, corresponding to the lithium and sodium storage capacity (≈ 96 mA hg^{-1} at 20 mVs^{-1}), are comparable. The high pseudocapacitance of LFP, which is more pronounced in $NaNO_3$ [16], contributes to that. However, at higher current rates (above 20 mV s^{-1}), the sodium capacity overtaking lithium's was not observed (faster increase of pseudocapacitance vs. diffusion with the scan rate increase) due to the material instability upon switching scan rates in $NaNO_3$.

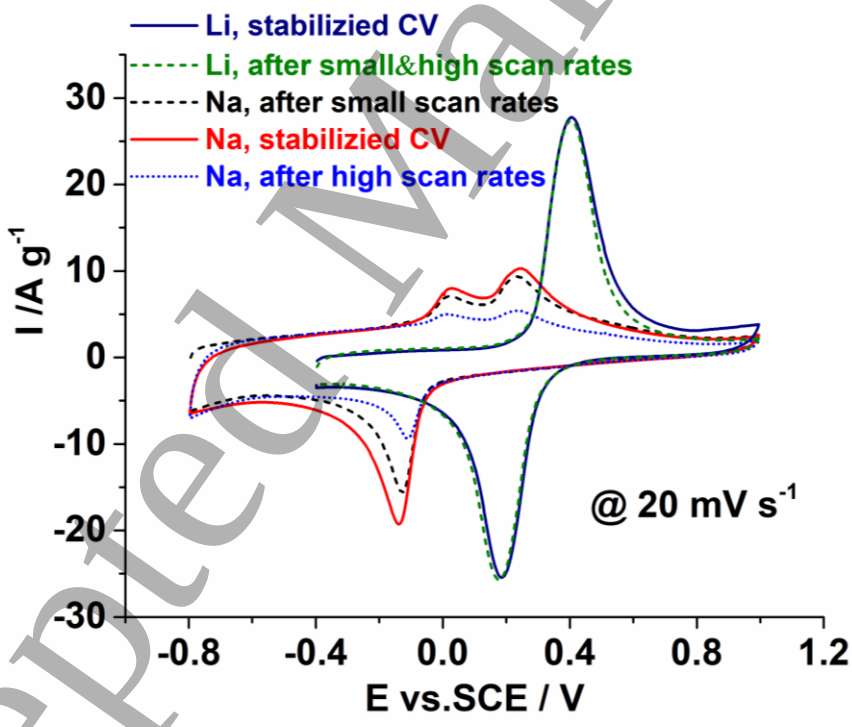

Figure 7. CVs of LFP/C-10V measured in $NaNO_3$ and $LINO_3$ aqueous electrolytes before (stabilized CV) and after lower (two cycles with 10, 5, 1 mV s^{-1}) and higher scan rates (two cycles with 50, 100, 150, 200, 300 m V s^{-1}).

Table 4. The specific coulombic capacity calculated from CV of LFVP/C in $NaNO_3$ electrolyte, at different scan rates.

Scan rate /mVs^{-1}	Anodic capacity / mAh g^{-1} (desodiation)	Cathodic capacity/ mAh g^{-1} (sodiation)
1	82	96
5	96	94
10	96	96
20	96	96
30	88	75
50	73	71
100	68	66
150	64	62
200	60	58

Although the material exhibits a high storage capacity for both lithium and sodium ions, it has less potential to be applied as a cathode for Na- than for Li-ion batteries due to its instability in $NaNO_3$. Otherwise, the good stability of LFP/C-10V was registered in $LiNO_3$. Interestingly, CV deterioration of olivine in $NaNO_3$ was not observed at low-level of vanadium doping (3mol% and 5mol%) [29], since the decrease in CV current was not observed after high scan rates. Since low-level doped samples have Fe_2P phase, which is not detected at high doping level of 10 mol%, we conclude that Fe_2P is favorable for cyclic stability of olivine.

4. Conclusions

$LiFe_{0.9}V_{0.01}PO_4$/13wt.%C composition was successfully synthesized via simple and fast gel-combustion route, at 750 ^oC in an Ar/H_2 atmosphere. Vanadium ions were incorporated into the targeted Fe^{2+} sites at 10mol%, which was followed by the formation of vacancies and surface $Li_3V_2PO_4$ traces. With heavy vanadium doping, the electrochemical performance of the composite is improved, especially at high current rates, due to an increased electronic conductivity ($\approx 1.43 \times 10^{-3} \rightarrow 2 \times 10^{-2}$ S cm^{-1}) and longer Li-O bonds (2.1341 → 2.1460 Å). By comparing the electrochemical performance of the composite with different vanadium doping levels, it can be seen that the capacity improvement follows the trend of an increasing vanadium content (0, 3 mol %, 5mol% and 10 mol%.). Namely, the optimal specific capacity of the composite was achieved at the highest doping level (10 mol%), where a fully reversible process was identified in $LiNO_3$ at 1mV s^{-1} as evidenced through the theoretical value of peak-to-peak separation ($\Delta Ep/2$=28mV). Therefore, LFP/C-10V composite delivers a high specific capacity not only in $LiNO_3$ (101/103 mAh g^{-1} for delithiation/lithiation), but also in $NaNO_3$ (96/96 mAh g^{-1} for desodiation/sodiation), making it one of the best cathode materials for aqueous batteries. However, the cycling at different scan rates only shows the stable behavior of the composite in $LiNO_3$, thus offering an advantage to this cathode material for Li-ion batteries. At high current rates of 100 C, the composite can retain the capacity value of around 50 mAh g^{-1} in $LiNO_3$.

Acknowledgments:
Authors acknowledge the Ministry of Science, Technological Development and Innovation of the Republic of Serbia for support through the national programme (Contract number: 451-03-66/2024-03/200146, 451-03-47/2023-01/200017, and 451-03-47/2023-01/200175), bilateral Serbia-India project (no.14, entitled "Developments of State of Health Monitoring Devices for Battery Management Systems in Electric Vehicles") and bilateral Serbia-Austria project (OeAD-GmbH-Project no. RS 24/2022) 337-00-577/2021-09/6).

5. References

[1] M. Marinaro, D. Bresser, E. Beyer, P. Faguy, K. Hosoi, H. Li, J. Sakovica, K. Amine, M. Wohlfahrt-Mehrens, S. Passerini, Bringing forward the development of battery cells for automotive applications: Perspective of R&D activities in China, Japan, the EU and the USA, J. Power Sources. 459 (2020) 228073. https://doi.org/10.1016/j.jpowsour.2020.228073.

[2] A. Eftekhari, On the Theoretical Capacity/Energy of Lithium Batteries and Their Counterparts, ACS Sustain. Chem. Eng. 7 (2019) 3684–3687. https://doi.org/10.1021/acssuschemeng.7b04330.

[3] A. Eftekhari, Lithium-Ion Batteries with High Rate Capabilities, ACS Sustain. Chem. Eng. 5 (2017) 2799–2816. https://doi.org/10.1021/acssuschemeng.7b00046.

[4] M. Armand, P. Axmann, D. Bresser, M. Copley, K. Edström, C. Ekberg, D. Guyomard, B. Lestriez, P. Novák, M. Petranikova, W. Porcher, S. Trabesinger, M. Wohlfahrt-Mehrens, H. Zhang, Lithium-ion batteries – Current state of the art and anticipated developments, J. Power Sources. 479 (2020). https://doi.org/10.1016/j.jpowsour.2020.228708.

[5] R. Article, Towards greener and more sustainable batteries for electrical energy storage, 7 (2015) 19-29. https://doi.org/10.1038/NCHEM.2085.

[6] A. Ponrouch, J. Bitenc, R. Dominko, N. Lindahl, P. Johansson, M.R. Palacin, Multivalent rechargeable batteries, Energy Storage Mater. 20 (2019) 253–262. https://doi.org/10.1016/j.ensm.2019.04.012.

[7] M. Vujković, Comparison of lithium and sodium intercalation materials, J. Serbian Chem. Soc. 80 (2015) 801–804. https://doi.org/10.2298/JSC141119127V.

[8] A. Gezović, M.J. Vujković, M. Milović, V. Grudić, R. Dominko, S. Mentus, Recent developments of $Na_4M_3(PO_4)_2(P_2O_7)$ as the cathode material for alkaline-ion rechargeable batteries: challenges and outlook, Energy Storage Mater. 37 (2021) 243–273. https://doi.org/10.1016/j.ensm.2021.02.011.

[9] A.K. Padhi, K.S. Nanjundaswamy, J.B. Goodenough, Journal of The Electrochemical Society, J. Electrochem. Soc. (1997) 1188–1193.

[10] A.K. Padhi, K.S. Nanjundaswamy, C. Masquelier, S. Okada, J.B. Goodenough, Effect of Structure on the Fe3 + / Fe2 + Redox Couple in Iron Phosphates, J. Electrochem. Soc. 144 (1997) 1609–1613. https://doi.org/10.1149/1.1837649.

[11] H. Zhu, C. Miao, R. Guo, Y. Liu, X. Wang, A Simple and Low-cost Synthesis Strategy of LiFePO4 Nanoparticles as Cathode Materials for Lithium Ion Batteries, Int. J. Electrochem. Sci. 16 (2021) 1–12. https://doi.org/10.20964/2021.03.27.

[12] Y. Wang, Y. Wang, E. Hosono, K. Wang, H. Zhou, The design of a LiFePO4/carbon nanocomposite with a core-shell structure and its synthesis by an in situ polymerization restriction method, Angew. Chemie - Int. Ed. 47 (2008) 7461–7465. https://doi.org/10.1002/anie.200802539.

[13] B. Lung-Hao Hu, F.Y. Wu, C. Te Lin, A.N. Khlobystov, L.J. Li, Graphene-modified $LiFePO_4$ cathode for lithium ion battery beyond theoretical capacity, Nat. Commun. 4 (2013) 1–7. https://doi.org/10.1038/ncomms2705.

[14] L. Guo, W. Wei, L. Guo, X. Qiu, P. Qu, M. Xu, Porous micro-spherical LiFePO4/CNT nanocomposite for high-performance Li-ion battery cathode material, RSC Adv. 5 (2015) 37830–37836. https://doi.org/10.1039/c5ra05988g.

[15] S.Y. Chung, J.T. Bloking, Y.M. Chiang, Electronically conductive phospho-olivines as lithium storage electrodes, Nat. Mater. 1 (2002) 123–128. https://doi.org/10.1038/nmat732.

[16] F. Omenya, N.A. Chernova, S. Upreti, P.Y. Zavalij, K.W. Nam, X.Q. Yang, M.S. Whittingham, Can vanadium be substituted into $LiFePO_4$?, Chem. Mater. 23 (2011) 4733–4740. https://doi.org/10.1021/cm2017032.

[17] C. Gao, J. Zhou, G. Liu, L. Wang, Synthesis of F-doped $LiFePO_4$/C cathode materials for high performance lithium-ion batteries using co-precipitation method with hydrofluoric acid source, J. Alloys Compd. 727 (2017) 501–513. https://doi.org/10.1016/j.jallcom.2017.08.149.

[18] J. Hong, C.S. Wang, X. Chen, S. Upreti, M.S. Whittingham, Vanadium modified LiFeP O4 Cathode for Li-ion batteries, Electrochem. Solid-State Lett. 12 (2009) 2–7. https://doi.org/10.1149/1.3039795.

[19] S. Jiang, Y. Wang, Synthesis and characterization of vanadium-doped LiFePO 4 @C electrode with excellent rate capability for lithium-ion batteries, Solid State Ionics. 335 (2019) 97–102. https://doi.org/10.1016/j.ssi.2019.03.002.

[20] I.D. Johnson, M. Lübke, O.Y. Wu, N.M. Makwana, G.J. Smales, H.U. Islam, R.Y. Dedigama, R.I. Gruar, C.J. Tighe, D.O. Scanlon, F. Corà, D.J.L. Brett, P.R. Shearing, J.A. Darr, Pilot-scale continuous synthesis of a vanadium-doped LiFePO4/C nanocomposite high-rate cathodes for lithium-ion batteries, J. Power Sources. 302 (2016) 410–418. https://doi.org/10.1016/j.jpowsour.2015.10.068.

[21] Z. Lu-Lu Zhang, Gan Liang,‡ Alexander Ignatov,§,Mark C. Croft, Xiao-Qin Xiong,† I-Ming Hung, and Y.-L.P. Yun-Hui Huang,* Xian-Luo Hu, Wu-Xing Zhang, Effect of vanadium doping on electrochemical performance of $LiFePO_4$ for lithium-ion batteries, J. Solid State Electrochem. 115 (2011) 13520–13527. https://doi.org/10.1007/s10008-013-2315-9.

[22] K.L. Harrison, A. Manthiram, Microwave-assisted solvothermal synthesis and

characterization of metastable $LiFe_{1-x}(VO)_xPO_4$ cathodes, Inorg. Chem. 50 (2011) 3613–3620. https://doi.org/10.1021/ic1025747.

[23] J. Ma, B. Li, H. Du, C. Xu, F. Kang, The Effect of Vanadium on Physicochemical and Electrochemical Performances of $LiFePO_4$ Cathode for Lithium Battery, J. Electrochem. Soc. 158 (2011) A26. https://doi.org/10.1149/1.3514688.

[24] K.L. Harrison, C.A. Bridges, M.P. Paranthaman, C.U. Segre, V.A. Maroni, J.C. Idrobo, J.B. Goodenough, Supporting Information Temperature Dependence of Aliovalent-vanadium Doping in $LiFePO_4$ Cathodes Katharine L. Harrison, Chem. Mater. 25 (2013) 768−781.

[25] J. Hong, X.L. Wang, Q. Wang, F. Omenya, N.A. Chernova, M.S. Whittingham, J. Graetz, Structure and electrochemistry of vanadium-modified $LiFePO_4$, J. Phys. Chem. C. 116 (2012) 20787–20793. https://doi.org/10.1021/jp306936t.

[26] C. Chiang, H. Su, P. Wu, H. Liu, C. Hu, N. Sharma, V.K. Peterson, H. Hsieh, Y. Lin, W. Chou, C. Lee, J. Lee, B. Shew, Vanadium Substitution of LiFePO 4 Cathode Materials To Enhance the Capacity of $LiFePO_4$ - Based Lithium-Ion Batteries, (2012).

[27] H. Lin, Y. Wen, C. Zhang, L. Zhang, Y. Huang, B. Shan, R. Chen, A GGAU study of lithium diffusion in vanadium doped LiFePO 4, Solid State Commun. 152 (2012) 999–1003. https://doi.org/10.1016/j.ssc.2012.03.027.

[28] M. Vujković, D. Jugović, M. Mitrić, I. Stojkovic, N. Cvjetićanin, S. Mentus, The $LiFe_{(1-x)}V_xPO_4$/C composite synthesized by gel-combustion method, with improved rate capability and cycle life in aeratedaqueous solutions, Electrochim. Acta. 109 (2013) 835–842. https://doi.org/10.1016/j.electacta.2013.07.219.

[29] M. Vujković, S. Mentus, Potentiodynamic and galvanostatic testing of $NaFe_{0.95}V_{0.05}PO_4$/C composite in aqueous $NaNO_3$ solution, and the properties of aqueous $Na_{1.2}V_3O_8$/$NaNO_3$/$NaFe_{0.95}V_{0.05}PO_4$/C battery, J. Power Sources. 325 (2016) 185–193. https://doi.org/10.1016/j.jpowsour.2016.06.031.

[30] M. Vujković, I. Stojković, N. Cvjetićanin, S. Mentus, Gel-combustion synthesis of $LiFePO_4$/C composite with improved capacity retention in aerated aqueous electrolyte solution, Electrochim. Acta. 92 (2013) 248–256. https://doi.org/10.1016/j.electacta.2013.01.030.

[31] H.M. Rietveld, A profile refinement method for nuclear and magnetic structures, J. Appl. Crystallogr. 2 (1969) 65–71. https://doi.org/10.1107/s0021889869006558.

[32] R.W. Cheary, A. Coelho, Fundamental parameters approach to x-ray line-profile fitting, J. Appl. Crystallogr. 25 (1992) 109–121. https://doi.org/10.1107/S0021889891010804.

[33] R.D. Shannon, Application of the Periodic Bond Chain (PBC) Theory and Attachment Energy Consideration to Derive the Crystal Morphology of Hexamethylmelamine, Pharm. Res. An Off. J. Am. Assoc. Pharm. Sci. 32 (1976) 751. https://doi.org/10.1023/A:1018927109487.

[34] N. Hua, C. Wang, X. Kang, T. Wumair, Y. Han, Studies of v doping for the LiFePO4-based Li Ion batteries, J. Alloys Compd. 503 (2010) 204–208.

https://doi.org/10.1016/j.jallcom.2010.04.233.

[35] C. Gao, J. Zhou, G. Liu, L. Wang, Lithium-ions diffusion kinetic in $LiFePO_4$/carbon nanoparticles synthesized by microwave plasma chemical vapor deposition for lithium-ion batteries, Appl. Surf. Sci. 433 (2018) 35–44. https://doi.org/10.1016/j.apsusc.2017.10.034.

[36] C.S. Sun, Z. Zhou, Z.G. Xu, D.G. Wang, J.P. Wei, X.K. Bian, J. Yan, Improved high-rate charge/discharge performances of $LiFePO_4$/C via V-doping, J. Power Sources. 193 (2009) 841–845. https://doi.org/10.1016/j.jpowsour.2009.03.061.

[37] P. Liu, Y. Zhang, P. Dong, Y. Zhang, Q. Meng, S. Zhou, X. Yang, M. Zhang, X. Yang, Direct regeneration of spent LiFePO4 cathode materials with pre-oxidation and V-doping, J. Alloys Compd. 860 (2021) 157909. https://doi.org/10.1016/j.jallcom.2020.157909.

[38] C. Shen, W. Lin, H. Hu, P. Yang, L. Wang, The electronic and geometric structure modifications of $LiFePO_4$ with vanadium doping to achieve ultrafast discharging capability: The experimental and theoretical investigations, J. Alloys Compd. 936 (2023) 168035. https://doi.org/10.1016/j.jallcom.2022.168035.

[39] C.D. Wagner, W.M. Riggs, L.E. Davis, J.F. Moulder, G.E. Muilenberg, Handbook of X-ray electron spectroscopy, Perkin-Elmer Corp. (1979) 192.

[40] J. Ma, B. Li, F. Kang, Improved electrochemical performances of nanocrystalline $LiFePO_4$/C composite cathode via V-doping and VO_2(B) coating, J. Phys. Chem. Solids. 73 (2012) 1463–1468. https://doi.org/10.1016/j.jpcs.2011.12.018.

[41] C. Shen, W. Lin, H. Hu, P. Yang, L. Wang, The electronic and geometric structure modifications of $LiFePO_4$ with vanadium doping to achieve ultrafast discharging capability: The experimental and theoretical investigations, J. Alloys Compd. 936 (2023) 168035. https://doi.org/10.1016/j.jallcom.2022.168035.

[42] P. Liu, Y. Zhang, P. Dong, Y. Zhang, Q. Meng, S. Zhou, X. Yang, M. Zhang, X. Yang, Direct regeneration of spent $LiFePO_4$ cathode materials with pre-oxidation and V-doping, J. Alloys Compd. 860 (2021) 157909. https://doi.org/10.1016/j.jallcom.2020.157909.

[43] R. Dominko, M. Bele, M. Gaberscek, M. Remskar, D. Hanzel, J.M. Goupil, S. Pejovnik, J. Jamnik, Porous olivine composites synthesized by sol-gel technique, J. Power Sources. 153 (2006) 274–280. https://doi.org/10.1016/j.jpowsour.2005.05.033.

[44] M. Vujković, M. Mitrić, S. Mentus, High-rate intercalation capability of $NaTi_2(PO_4)_3$/C composite in aqueous lithium and sodium nitrate solutions, J. Power Sources. 288 (2015) 176–186. https://doi.org/10.1016/j.jpowsour.2015.04.132.

[45] P. He, J.L. Liu, W.J. Cui, J.Y. Luo, Y.Y. Xia, Investigation on capacity fading of $LiFePO_4$ in aqueous electrolyte, Electrochim. Acta. 56 (2011) 2351–2357. https://doi.org/10.1016/j.electacta.2010.11.027.

[46] Y. Fang, Q. Liu, L. Xiao, X. Ai, H. Yang, Y. Cao, High-Performance Olivine $NaFePO_4$ Microsphere Cathode Synthesized by Aqueous Electrochemical Displacement Method for Sodium Ion Batteries, ACS Appl. Mater. Interfaces. 7 (2015) 17977–17984. https://doi.org/10.1021/acsami.5b04691.

[47] M. Vujković, S. Mentus, Fast sodiation/desodiation reactions of electrochemically delithiated olivine LiFePO4 in aerated aqueous $NaNO_3$ solution, J. Power Sources. 247 (2014) 184–188. https://doi.org/10.1016/j.jpowsour.2013.08.062.

[48] M. Casas-Cabanas,V. Roddatis, D. Saurel, P. Kubiak, J. Carretero-González, Verónica Palomares, P. Serras, Teófilo Rojo, Crystal chemistry of Na insertion / deinsertion in $FePO_4$ – $NaFePO_4$, J. Mater. Chem. 22 (2012) 17421–17423. https://doi.org/10.1039/c2jm33639a.